Coupling of remote sensing, field campaign, and mechanistic and empirical modeling to monitor spatiotemporal carbon dynamics of a Mediterranean watershed in a changing regional climate

S. Berberoglu · C. Donmez · F. Evrendilek

Abstract The aim of this study was to simulate impacts of regional climate change in the 2070s on carbon (C) cycle of a Mediterranean watershed combining field measurements, Envisat MERIS and IKONOS data, and the Carnegie Ames Stanford Approach model. Simulation results indicated that the present total C sink status (1.36 Mt C year^{-1}) of Mediterranean evergreen needleleaf forest, grassland and cropland ecosystems is expected to weaken by 7.6 % in response to the climate change in the 2070s (Mt=10^{12} g). This decreasing trend was mirrored in soil respiration (R_H), aboveground and belowground net primary production (NPP), NEP, and net biome production (NBP). The decrease in NEP in the 2070s was the highest (21.9 %) for mixed forest where the smallest present C sink of 0.03 Mt C year^{-1} was estimated. The average present net ecosystem production (NEP) values were estimated at 110±15, 75±19, and 41±25 g C m^{-2} years^{-1} in forest, grassland, and cropland, respectively, with a watershed-scale mean of 95± 30 g C m^{-2} years^{-1}. The largest present C sink was in grassland, with a total C pool of 0.55 Mt C year^{-1}, through its greater spatial extent.

Introduction

Human-induced alteration of local carbon (C) cycle across the world has cumulatively led to global climate change which in turn triggers a domino effect on ecosystem structure and function (Wali et al. 1999; Evrendilek 2014). Arid and semi-arid lands including Mediterranean ecosystems cover 30 to 45 % of the global terrestrial surface (Asner et al. 2003) and can be particularly considered to be the hot spots of the world associated with climate change due to their increasing potential for desertification and C sequestration. Interconnectedness and interdependencies of biogeochemical cycles and ecosystem compartments require that preventive and mitigative measures be taken towards sustainability of ecosystem services such as food/feed production, and climatic/hydrological regulation at the local and regional scales (Lobell et al. 2002; Jian-Bing et al. 2006; Pandey et al. 2011). One of the main foci in the related literature has been not only on the quantification of feedbacks between C cycling and climate change for a better understanding but also on the integration of spatially and temporally explicit process-based models, data-driven models, remote sensing, and geographical information systems (GIS) for continuous monitoring.

S. Berberoglu · C. Donmez
Division of Remote Sensing and GIS, Department of Landscape Architecture, Cukurova University, Adana, Turkey

F. Evrendilek (✉)
Department of Environmental Engineering, Abant Izzet Baysal University, Bolu, Turkey
e-mail: fevrendilek@ibu.edu.tr

Process-based simulations coupled with remotely sensed data and GIS have enhanced the environmental capability of monitoring spatiotemporal dynamics of C cycle. This integration offers an essential tool to repetitively acquire environmental data at spatial, temporal, radiometric, and spectral resolutions appropriate to quantify patterns of human alterations of C cycling. Process-based biogeochemical models can be classified into: (1) remote sensing-based models such as Carnegie Ames Stanford Approach (CASA) model (Potter et al. 1993), GLObal Production Efficiency Model (GLO-PEM) (Prince and Goward 1995), Simple Diagnostic Biosphere Model (SDBM) (Knorr and Heimann 1995), Simple Interactive Biosphere model (SIB2) (Sellers et al. 1996), and Terrestrial Uptake and Release of Carbon model (TURC) (Ruimy et al. 1996); (2) models that simulate coupled biogeochemical cycles of C, nitrogen (N), phosphorus (P), sulfur (S) or water (H_2O) using a prescribed vegetation classification system such as Biome BioGeochemical Cycle (BIOME-BGC) model (Running et al. 2004), CENTURY model (Parton et al. 1993), and The Terrestrial Ecosystem Model (TEM) (McGuire et al. 2001); and (3) models that simulate dynamics of both plant functional types and coupled biogeochemical cycles such as Global Biome (BIOME3) model (Haxeltine and Prentice 1996), Dynamic Global Phytogeography model (Woodward et al. 1995), ORCHIDEE model (Krinner et al. 2005), and LPJ-GUESS model (Hickler et al. 2004).

Despite these advances, the magnitude, distribution, and dynamics of global C sinks and sources remain still uncertain. One of the main reasons for this may be associated with monitoring of local C sinks and sources disproportionately across ecosystems at too coarse or too fine spatiotemporal resolutions (Running et al. 1999; Barford et al. 2001; Schnell et al. 2014). Adoption of watershed-scale monitoring, modeling, mapping, and management may facilitate to bridge differences between leaf- and globe-scale quantifications of biogeochemical dynamics. One of the understudied biomes in terms of C cycle is the Mediterranean watersheds in Turkey as well as globally. The Mediterranean ecosystems are relatively more vulnerable to effects of climate change due to their exposure to semi-arid conditions and severe and prolonged human-induced pressures. There is a lack of experimental studies about as well as a pressing need for model simulations at a relatively fine spatial scale for such under-sampled Mediterranean

ecosystems through the coupling of regionally down-scaled future (2070s) climate (temperature and rainfall) projections, remotely sensed data, field campaigns, and process-based (mechanistic) and data-driven (empirical) modeling. The objective of this study was, therefore, to quantify impacts of regional climate change in the 2070s on C cycle of an upper Mediterranean watershed synthesizing field measurements, remote sensing data, and the CASA model.

Materials and methods

Description of study region

The upper Seyhan watershed is located in the Taurus Mountain range of the southern Mediterranean region of Turkey and covers ca. 18,311 km² (Fig. 1). Dominant forest cover of the study region is characterized by old-growth Mediterranean evergreen needleleaf forest with pure and mixed stands of the following dominant tree species: Crimean pine (*Pinus nigra*), Lebanese cedar (*Cedrus libani*), Taurus fir (*Abies cilicica*), Turkish pine (*Pinus brutia*), and Juniper (*Juniperus excelsa*) (Evrendilek et al. 2006). Mixed forest is generally composed of *P. brutia* and *P. nigra*; *P. brutia* and *J. excelsa*; *P. nigra* and *A. cilicica*; and *C. libani* and *A. cilicica* stands. Mild and rainy winters and hot and dry summers are typical across the study region with a mean annual rainfall (MAP) of about 800 mm 75 % of which are received in autumn (September to November) and winter (December to March). Mean annual air temperature (MAT) is 19 °C with mean minimum and maximum values of 8 °C in January and 30 °C in July, respectively. Dominant soil types of the upper Seyhan watershed are leptosols for grasslands and forests and fluvisols/vertisols for croplands (Eswaran et al. 2011). The two main soil texture categories of clay loam and light clay cover 54 and 42 % of the study region, respectively (Eswaran et al. 2011).

Climate, remotely sensed, and ancillary data

Long-term climate data (1993–2004) of monthly rainfall, air temperature, and solar radiation were compiled from 50 weather stations across the Seyhan watershed so as to represent the present regional climate conditions. The geostatistical interpolation of co-kriging was used to map the climate variables on a monthly basis
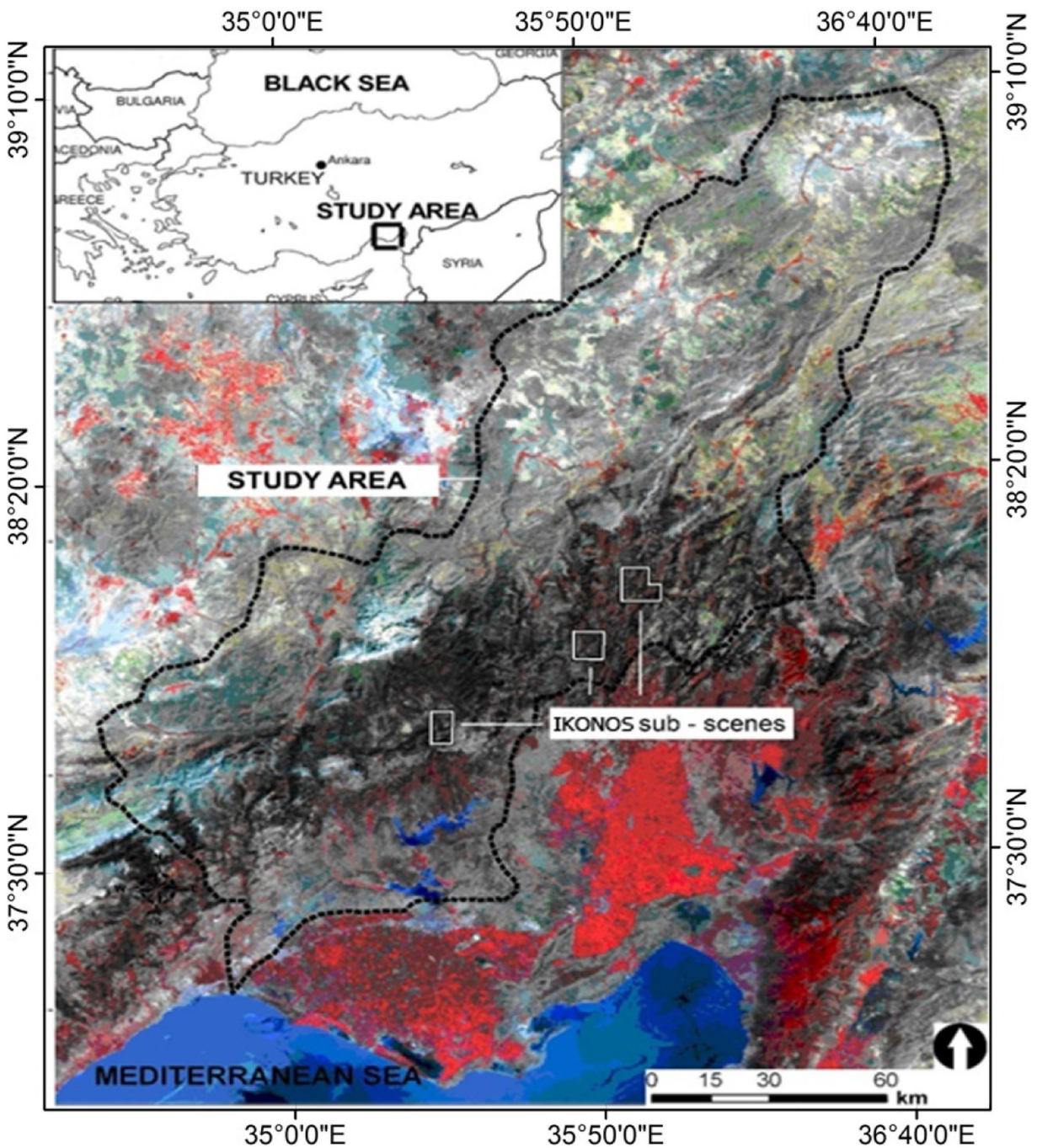
Fig. 1 Envisat MERIS image of the upper Seyhan watershed (coordinates in meters)

using digital elevation model (DEM). Kimura et al. (2007) provided regional *pseudo warming* data for the 2070s (2071 to 2080) in accordance with A2 scenario (medium-high emissions from a continuously increasing global population) and AR3 climate model outputs of IPCC (2000). In so doing, a Regional Climate Model (RCM) was used to downscale the General Circulation Models (GCMs) due to the coarse spatial resolution of GCMs, given the study region. The forcing data for the boundary conditions of the RCM were given by the Meteorological Research Institute in Japan (MRI).

Envisat MERIS and IKONOS were utilized as remotely sensed data in this study. Envisat MERIS data acquired consisted of 47 images from March 2003 to September 2005 (Fig. 2). Monthly NDVI images were derived from bands 10 and 6 of the 47 Envisat MERIS images and were inputted into the CASA model. The NDVI map (Fig. 3) was used originally to generate vegetation distribution map of the study area and enabled the model to differentiate ecosystem types to quantify watershed-scale NPP. Using NDVI data,

phenological characteristics of the land cover types were also defined and extracted which in turn assisted in the modeling procedure.

Three sub-scenes of multispectral IKONOS imagery representing different types of forest cover recorded in May 2002 were used in training and testing for percentage tree cover estimates. Soil texture designations as coarse, medium, or fine were assigned to the top 30 cm of soil using the classification system of Food and Agriculture Organization (FAO), and a soil map of
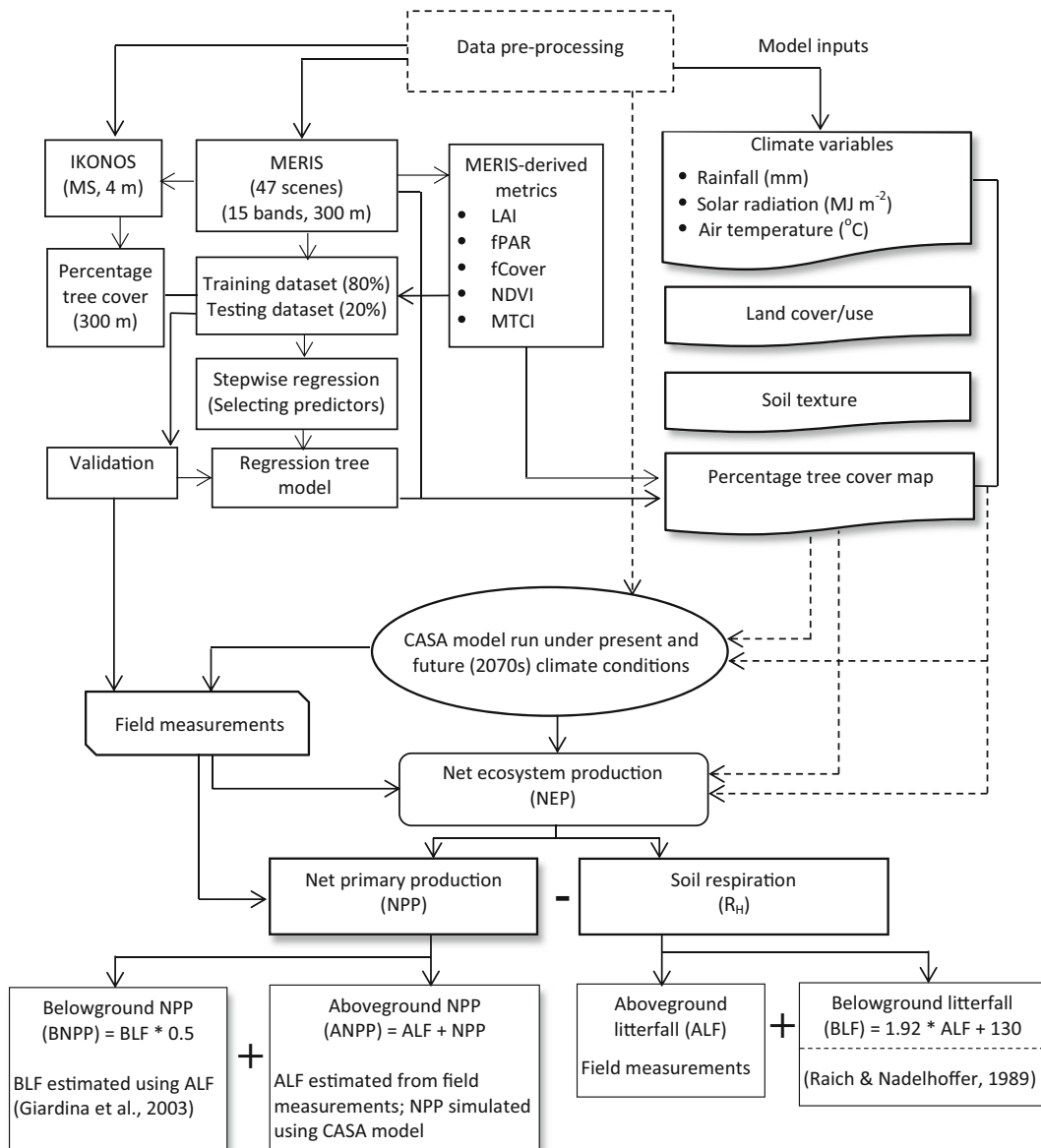

Fig. 2 A flow diagram depicting the methodology adopted in this study for prediction of watershed-scale impacts of regional climate change in the 2070s on C cycle
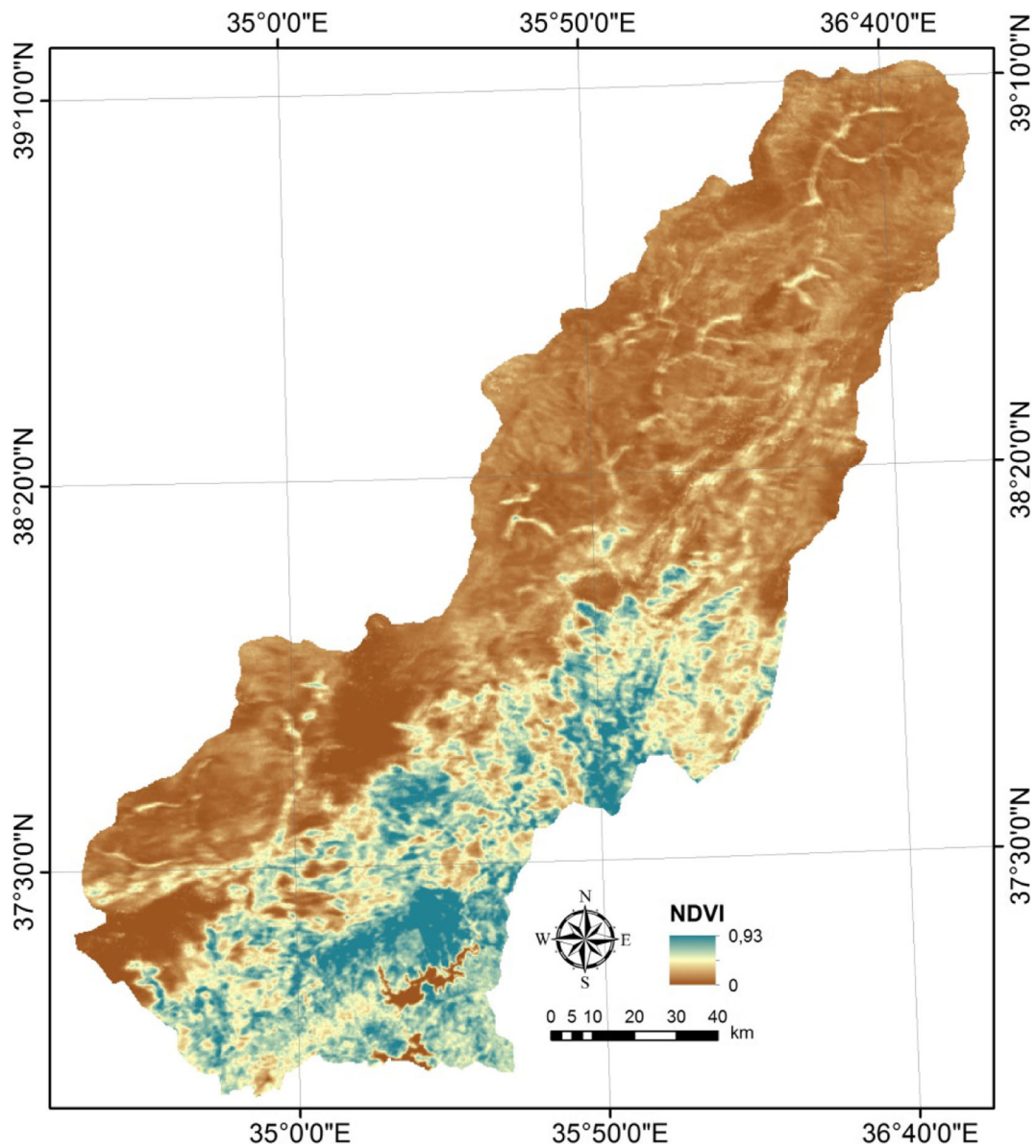
Fig. 3 Normalized Difference Vegetation Index (NDVI) map of the upper Seyhan watershed

1:25,000 scale. Forestry and topographic maps, and aerial photographs at the scale of 1:25,000 were also used in the analysis together with climate data.

Land cover/use classification

Land cover/use classification was generated using ERDAS imagine (version 9.1) and was based on Landsat ETM image for 17 August 2003, DEM, land cover records of State Hydraulic Works (DSI), and field measurements. The Landsat ETM image was geometrically corrected and geocoded to the Universal Transverse Mercator (UTM) coordinate system by using a topographic map of 1:25,000 scale. The maximum likelihood algorithm with supervised training was used for image classification (Fig. 2). The initial classification carried out differentiated among 27 land cover/use classes at a 30-m spatial resolution and was altered to represent the following seven classes: (1) mixed forest, (2) *P. brutia*, (3) *P. nigra*, (4) *C. libani*, (5) *J. excelsa*, (6) grassland, and (7) cropland. Water bodies and urban surfaces were masked out. The maps generated were

then rasterized to a 30-m cell size using the nearest neighbor algorithm.

Percentage tree cover

Percentage tree canopy cover was estimated using the following five steps: (1) generation of a reference dataset for percentage tree cover; (2) derivation of metrics from Envisat MERIS data; (3) selection of predictor variables; (4) fitting regression tree (RT) models; and (5) accuracy assessment (Donmez et al. 2015) (Fig. 2). A reference dataset for percentage tree cover was generated using multispectral IKONOS images at a 4-m spatial resolution to train the model. Three sub-scenes of IKONOS images were selected to represent different forest cover types and were classified as tree and non-tree pixels over an area of 120 km^2. Classification results were then used to estimate percentage tree cover at the spatial resolution of MERIS.

Fifteen spectral bands of Envisat MERIS data (390 to 1040 nm), NDVI, leaf area index (LAI), fraction of photosynthetically active radiation (fPAR), fraction of green vegetation cover per a unit area of horizontal soil (fCover), and MERIS terrestrial chlorophyll index (MTCI) were used as biophysical predictors in the model. The ratio of reflectance difference between bands 10 and 9 to reflectance difference between bands 9 and 8 for Envisat MERIS is defined as MTCI (Dash and Curran 2006). Using the top of canopy land products algorithm (TOA_VEG version 3) developed by Weiss et al. (2006), LAI, fPAR, and fCover were estimated through the visualization and analyzing tool of the MERIS/(A)ATSR Toolbox (VISAT). A stepwise linear regression (SLR) method was used for the addition to RT model of the most significant predictors that explain percentage tree cover (Helsel and Hirsch 1992). The entire IKONOS data were partitioned into training (1023 pixels) and testing (209 pixels) datasets. After the geometric and radiometric corrections of the IKONOS images, four models built using the SLR method were trained with the reference data derived from the IKONOS images. Relationships between percentage tree cover and spectral values of Envisat MERIS were modeled using the RT model. Finally, the predictive performance of the RT model was assessed comparing estimated versus measured values of percentage tree cover.

Aboveground litterfall

Monthly aboveground litterfall was collected from five forest stands. For sampling of forest litterfall, the following forest stands with the highest canopy cover were selected so as to best represent local forest conditions: *P. nigra*, *C. libani*, *P. brutia*, *J. excelsa* and mixed forest stands. Litterfall was sampled using five permanent circular litterfall traps of 0.20 m^2 per each stand. The individual traps at each site were set up for sampling on 17 June, 25 July, 20 September, 23 October, 17 November, and 24 December 2004. The composite samples were sorted into pine needles, small woody materials (e.g., bark, wood, and branches <1 cm diameter), reproductive structures (e.g., flowers, fruits, and cones), and unclassified materials (e.g., any material passing through a 2-mm sieve). The samples were weighed after being oven-dried at 70 °C for 48 h until a constant dry weight (DW) content was achieved. Aboveground litterfall addition to the soil from the evergreen needleleaf forest was expressed in C units using the ratio of 0.45 for the conversion of DW to C content (Evrendilek et al. 2006). Relationship between maximum canopy cover and litterfall explored for each forest type in different seasons showed that the litterfall measurements were strongly correlated with canopy cover, species, and season. Thus, the field measurements linked with canopy cover and land cover map were used to determine the spatial distribution of aboveground litterfall over the entire study region.

Soil respiration

Soil respiration is defined as total CO_2 efflux from soils as a function of decomposition and mineralization of soil organic matter by soil microorganisms and autotrophic respiration of plant roots (Raich and Schlesinger 1992). As with NPP, R_H is a major component of C cycle and can be assumed to equal above- and belowground litter inputs at a steady state thus (Kirschbaum 1995):

$$R_H = ALF + BLF \qquad (1)$$

where BLF was estimated for mature forests as a function of ALF (g C m^{-2} years^{-1}) based on the

following least square regression model (Raich and Nadelhoffer 1989):

$$BLF = 130 + 1.92 \times ALF \qquad (2)$$

Net primary production

Monthly NPP was estimated using the CASA model as a function of downwelling PAR, NDVI, light use efficiency (ε), fPAR, and reduction factors as follows:

$$NPP = f(fPAR \times \varepsilon \times g(T) \times h(W)) \qquad (3)$$

where fPAR (MJ m^{-2} month^{-1}) is a function of NDVI and downwelling PAR. Light use efficiency (g C MJ^{-1}) is a potential ε value adjusted by such reduction factors as temperature effect—$g(T)$—and water stress—$h(W)$—(Potter et al. 2003).

Net ecosystem production

Net ecosystem production (g C m^{-2} years^{-1}) was estimated as follows:

$$NEP = (ANPP + BNPP) - R_H \qquad (4)$$

For a better quantification of NEP for the land cover/use types under regional climate change, the following maps were generated at a 300-m resolution: (1) aboveground litterfall (ALF); (2) belowground litterfall (BLF); (3) R_H; and (4) aboveground and belowground NPP (ANPP and BNPP). Half of BLF was assumed to equal BNPP which was in turn added to ANPP to estimate total NPP (Giardina et al. 2003) (Fig. 2).

Results and discussion

Land cover/use classification

The accuracy assessment of the classification was carried out using the systematic sampling method. First, a total of 500 samples as the reference data were collected using GPS from the study area. Second, the class types were determined at the specific locations based on ground-truth data. Finally, a comparison of the class types determined using the reference data versus those of the classified map was quantified using an error matrix for the accuracy of the classification presented in Table 1. Overall accuracy derived from the stratified random sampling method image was 94 % for the classified image with an overall kappa statistic of 85 %, the proportion of agreement discounting what is expected by chance alone.

Aboveground litterfall

The spatial distribution of aboveground litterfall for each forest type was interpolated over the study region as a linear function of percentage tree cover. The C input to the soil from aboveground litterfall was assumed to reflect the maximum rates since the sampling plots for litterfall were representative of the Mediterranean evergreen needleleaf forest with the highest fractional canopy cover. Similarly, Matala et al. (2008) reported a significant linear relationship between litterfall (kg ha^{-1}) and basal area (m^{-2} ha^{-1}) (r=0.84; p<0.01). The best-fit MLR models of aboveground litterfall as a function of NPP, rainfall, and solar radiation were presented in Table 2.

Annual aboveground litterfall across the study region was estimated to vary between 1.5 Mg C ha^{-1} for *P. nigra* and *C. libani* and 4.3 Mg C ha^{-1} for grassland under the present climate and between 1.0 Mg C ha^{-1} for *C. libani* and 4.1 Mg C ha^{-1} for grassland under the climate change in the 2070s (Mg=10^6 g). Our findings were consistent with the European and Asian dry forests which were reported to add litterfall to the soil annually in the range of 0.78 to 3.4 Mg C ha^{-1} (n=19) and of 0.45 to 4.7 Mg C ha^{-1} (n=20), respectively (Chun-Jiang et al. 2003). Future aboveground litterfall predictions for the climate change in the 2070s based on the MLR models showed a general decrease over the entire watershed except for *J. excelsa* (Table 3). The rate of decrease in aboveground litterfall estimated in response to the projected climate change was the highest (35 %) for *C. libani*. Spatiotemporal changes in C input from aboveground litterfall to the soils of the terrestrial Mediterranean ecosystems between the present and future climate conditions are presented in Fig. 4a at a 300-m spatial resolution. Total aboveground litterfall for the upper watershed declined by 7.2 % from 5.7 to 5.3 Mt C year^{-1} under the climate change in 2070s (Mt=10^{12} g). Chun-Jiang et al. (2003) quantified that total aboveground litterfall values of 9±4.5 Mt C and 54±22.5 Mt C were transferred annually from the Asian and European dry forests to the soils, respectively.

Table 1 Accuracy assessment statistics of land cover/use classification

Class types	Producer's accuracy (%)	User's accuracy (%)	Kappa (%)
Water body	100	100	100
Rainfed agriculture	95	98	98
Irrigated agriculture	98	93	92
Bare ground	98	98	97
Grassland	100	100	100
Needleleaf forest	88	100	100
Deciduous forest	81	95	95
Total accuracy (%)	94		85

Soil respiration

Mean R_H rates of the terrestrial Mediterranean ecosystems across the study region under the present climate conditions ranged from 292±168 g C m^{-2} years^{-1} for cropland to 998±255 g C m^{-2} years^{-1} for *P. brutia*, with an overall mean R_H of 696±221 g C m^{-2} years^{-1}. From a total of 88 flux sites (19 sites from ChinaFLUX, 37 sites from AsiaFlux and 32 other sites), mean ecosystem respiration (R_E) of the Asian terrestrial ecosystems was derived as 990±827 g C m^{-2} years^{-1} (Chen et al. 2013). The mean R_H estimates of the Mediterranean terrestrial ecosystems in this study and the Asian terrestrial ecosystems appear to be consistent as the Asian R_E rate is the sum of both R_H and autotrophic respiration (R_A).

Raich and Schlesinger (1992) estimated mean annual R_H rates of 713±88 g C m^{-2} years^{-1} for Mediterranean woodlands (n=13) and 544±80 g C m^{-2} years^{-1} for croplands (n=26). Luyssaert et al. (2007) reported a mean R_H rate of 574±98 g C m^{-2} years^{-1} for Mediterranean evergreen forest. Meta-analysis by Wang and Fang (2009) indicated mean annual R_H rates of 389.8±45.5 and 601.3±45.6 g C m^{-2} years^{-1} for temperate and tropical grasslands, respectively. As in close agreement with the present study, long-term eddy covariance measurements from 2001 to 2008 over an open grassland in California (USA) under a Mediterranean climate (MAP=559 mm; MAT=16.3 °C) showed that R_H rates estimated from a carbon model (Ecosys) varied between 397 g C m^{-2} years^{-1} in 2008 and 685 g C m^{-2} years^{-1} in 2005, with a mean of 508±95 g C m^{-2} years^{-1} (Grant et al. 2012). As very close to the mean annual R_H rate of cropland in this study (292±168 g C m^{-2} years^{-1}), Ciais et al. (2010) reported a mean annual R_H rate of 299 g C m^{-2} years^{-1} over the EU-25 croplands.

Soil respiration rates across the study region under the climate change in the 2070s were, on average, found to decrease by 9 % and varied between 279±167 g C m^{-2} years^{-1} for cropland and 893±310 g C m^{-2} years^{-1} for *P. brutia* (Table 4). The decrease in R_H relative to the present period in response to the climate change in the 2070s ranged from 3 % for *J. excelsa* to 22 % for mixed forest. Similarly, meta-analysis by Wang et al. (2014), on average, showed a 16 % reduction in R_H across Mediterranean ecosystems (n=3) versus a 12 % increase in R_H across tundra, alpine, boreal, and temperate ecosystems in response to global warming by 2 °C, suggesting that increased temperature alone exerts an opposing effect on R_H in colder versus warmer climate.

Table 2 Multiple linear regression (MLR) models of annual aboveground litterfall (ALF, g C m^{-2} years^{-1}) for five Mediterranean forest types in the upper Seyhan watershed as a function of net primary production (NPP, g C m^{-2} years^{-1}), rainfall (RF, mm year^{-1}), and solar radiation (SR, MJ year^{-1})

Forest types	r^2_{adj} (%)	MLR models
Pinus brutia	69.1	ALF=405+0.251NPP−1.92RF+4.81SR
Pinus nigra	64.5	ALF=228+0.100NPP−4.83RF−2.00SR
Cedrus libani	74.0	ALF=200+0.0217NPP+10.7RF+25.0SR
Juniperus excelsa	72.9	ALF=100+0.382NPP−1.94RF+1.57SR
Mixed forest	75.2	ALF=168+0.174NPP−6.64RF−6.24SR

Table 3 Mean annual estimates of C inputs from belowground litterfall to forest, cropland and grassland soils under the present and future (the 2070s) regional climate conditions over the upper Seyhan watershed

Land cover/use types	Area (km²)	Present climate		Climate change in the 2070s		Change in litterfall (%)
		Litterfall (Mg C ha⁻¹ year⁻¹)	Total C (Mt C year⁻¹)	Litterfall (Mg C ha⁻¹ year⁻¹)	Total C (Mt C year⁻¹)	
Pinus brutia	1834	3.5±0.1	0.63	2.9±0.1	0.54	−15.6
Pinus nigra	713	1.5±0.2	0.11	1.4±0.1	0.10	−5.9
Cedrus libani	334	1.5±0.1	0.05	1.0±0.1	0.03	−35.3
Juniperus excelsa	610	1.8±0.1	0.11	2.0±0.1	0.13	9.8
Mixed forest	1517	1.7±0.2	0.26	1.5±0.2	0.23	−13.2
Cropland	5918	2.3±0.2	1.34	2.2±0.2	1.28	−4.0
Grassland	7385	4.3±0.4	3.22	4.1±0.3	3.00	−6.3

Aboveground and belowground net primary production

Monthly NPP was simulated as a function of temperature, rainfall, solar radiation, percentage tree cover, land cover/use map, soil texture, and NDVI under the present and future climate conditions and mapped at a 300-m spatial resolution (Fig. 4b). Present and future total NPP estimates ranged from 333 g C m⁻² years⁻¹ for cropland to 1134 g C m⁻² years⁻¹ for *P. brutia* and from 216 g C m⁻² years⁻¹ for cropland to 711 g C m⁻² years⁻¹ for *P. brutia*, respectively. Simulations of the CASA model provided watershed-scale mean NPP estimates of 792± 251 g C m⁻² years⁻¹ (553+239 g C m⁻² years⁻¹ for ANPP and BNPP) and 718±225 g C m⁻² years⁻¹ (500+ 218 g C m⁻² years⁻¹ for ANPP and BNPP) under the present and future climate conditions, respectively. A comparison of inventory-, site study- and vegetation model-based approaches for the EU-25 forests by Luyssaert et al. (2010) indicated total NPP estimates ranging from 439±176 g C m⁻² years⁻¹ by the BIOME-BGC model (White et al. 2000) to 638±255 g C m⁻² years⁻¹ for the modified LPJ-DGVM model (Zaehle et al. 2006). Ciais et al. (2010) reported an average estimate of the EU-25 cropland NPP ranging from 419 g C m⁻² years⁻¹ based on MODIS-2007 (Zhao et al. 2005) to 846 g C m⁻² years⁻¹ based on the FAO statistics and Haberl factors (Haberl et al. 2007).

Mean watershed-scale estimates of ANPP and BNPP for this study under the present climate conditions were 641±88 and 275±36 g C m⁻² years⁻¹ for evergreen needleleaf forest; 227±135 and 106±55 g C m⁻² years⁻¹ for cropland; and 435±73 and 191± 39 g C m⁻² years⁻¹ for grassland, respectively (Table 3). As consistent with our estimates, Luyssaert et al. (2007) estimated total NPP of Mediterranean evergreen forest at 801 g C m⁻² years⁻¹ (523 g C m⁻² years⁻¹ for ANPP and 278 g C m⁻² years⁻¹ for BNPP). According to Ruimy et al. (1994) and Lieth and Whittaker (1975), mean annual total NPP estimates per biome were 300 and 650 g C m⁻² years⁻¹ for Mediterranean closed forest; 470 and 300 g C m⁻² years⁻¹ for temperate grasslands; and 1000 and 300 g C m⁻² years⁻¹ for cultivation, respectively. Knapp et al. (2006) estimated mean ANPP values of climatically similar grasslands at 461±133 g m⁻² years⁻¹ for the Konza Prairie Biological Station in northeastern Kansas (USA) (MAP=857 mm; MAT=12.8 °C based on 43-year data) based on 15-year data and at 423±102 g m⁻² years⁻¹ for the Ukulinga Research Farm in Ukulinga (South Africa)
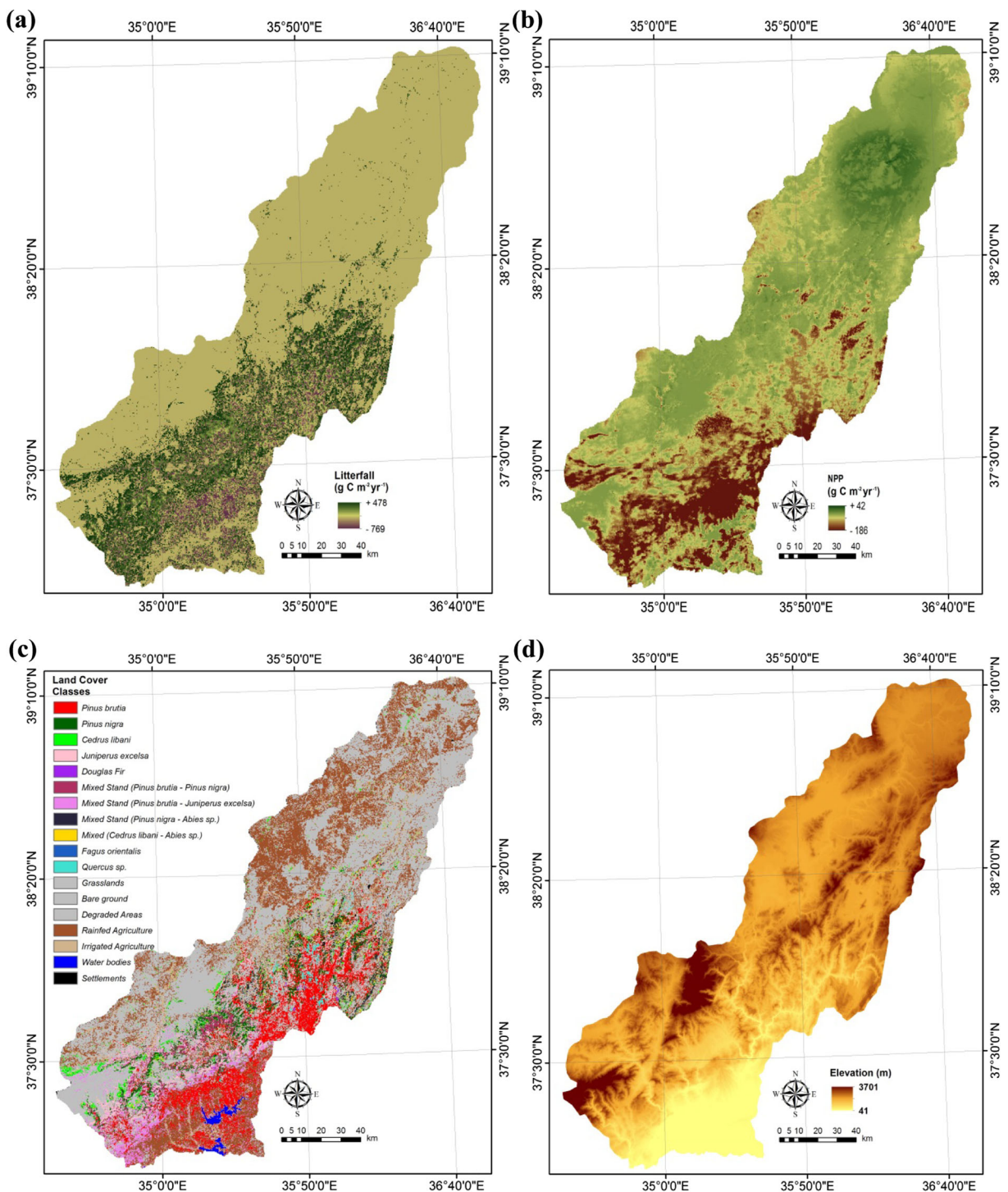
Fig. 4 Mapping of future changes in 2070 in **a** total litterfall (g C m^{-2} years^{-1}) and **b** total NPP (g C m^{-2} years^{-1}) in relation to **c** land cover/use classification, and **ds** digital elevation model (DEM) across the upper Seyhan watershed relative to the present regional climate conditions

(MAP=838 mm; MAT=18.6 °C based on 43-year data) based on 24-year data. After studying 15 stands of pine,

15 stands of oak, and 9 stands of mixed pine–oak between 2008 and 2011 in northeastern Portugal

(MAP=984 mm; MAT=13.5 °C), Nunes et al. (2013) found mean ANPP values to be 350, 320, and 540 g C m^{-2} years^{-1}, respectively.

Total NPP of the terrestrial Mediterranean ecosystems in this study decreased due to the regional climate change in the 2070s least for *J. excelsa* (-29 g C m^{-2} years^{-2}) and most for the mixed forest (-183 g C m^{-2} years^{-2}) (Table 4). Spatiotemporal dynamics in Fig. 4b show large areas of decreased levels of total NPP, especially, across the southern parts of the watershed, and small areas of increased levels of total NPP in the northern part. The maximum annual increase and decrease in total NPP in the 2070s are expected to occur in the evergreen needleleaf forest (42 g C m^{-2} years^{-2}) and in cropland and grassland (-186 g C m^{-2} years^{-2}), respectively (Fig. 4b). Simulated NPP patterns over the watershed under the present and future climate conditions indicated solar radiation, rainfall, and NDVI as the major drivers of variations in the growing season values of ANPP and BNPP. In the related literature, the main controls over globally spatial variations in NPP were reported to be fractional PAR absorption and biome-dependent light use efficiency (Field et al. 1995; Goetz et al. 1999). On the watershed scale, spatiotemporal NPP patterns are largely dependent on interactions among climate (e.g., rainfall, and PAR), biological processes (e.g., succession, species composition, herbivory, and nutrient uptake), and regimes of human-induced disturbances (e.g., climate change, air, water and soil pollution, urban sprawl, deforestation, over-grazing, and land cover/use conversions).

Net ecosystem production

All the Mediterranean ecosystems of the study region were net C sinks under the present and future climate conditions, with a net ecosystem sequestration rate ranging from 41±25 g C m^{-2} years^{-1} for cropland to 136±43 g C m^{-2} years^{-1} for *P. brutia* with an overall mean NEP of 95±30 g C m^{-2} years^{-1} (0.95±0.3 Mg C ha^{-1} year^{-1}) (Table 3). Hollinger et al. (2004) reported an overall mean NEP of 3±1 Mg C ha^{-1} year^{-1} for forests of the USA and Japan. Chen et al. (2013) stated that NEP of the Asian terrestrial ecosystems ranged from -150 g C m^{-2} years^{-1} (as a net source) to 1000 g C m^{-2} years^{-1} (as a net sink) with an overall mean NEP of 232±213 g C m^{-2} years^{-1} (the negative sign denotes a flux from ecosystems into the atmosphere).

Table 4 Mean annual estimates of soil respiration (R_H), aboveground net primary production (ANPP), belowground net primary production (BNPP), and net ecosystem production (NEP) of forests, cropland, and grassland across the upper Seyhan watershed under the present and future (the 2070s) regional climate conditions

Land cover/use type	Area (km²)	Under current regional climate conditions					Under regional climate change in 2070					Change in NEP (%)
		BNPP (g C m^{-2} years^{-1})	ANPP (g C m^{-2} years^{-1})	R_H (g C m^{-2} years^{-1})	NEP (g C m^{-2} years^{-1})	Total C pool (Mt C year^{-1})	BNPP (g C m^{-2} years^{-1})	ANPP (g C m^{-2} years^{-1})	R_H (g C m^{-2} years^{-1})	NEP (g C m^{-2} years^{-1})	TotalC pool (Mt C year^{-1})	
Pinus nigra	713	251±73	583±178	734±221	100±40	0.07	232±65	537±160	677±198	92±34	0.06	−7.7
Pinus brutia	1834	338±84	796±206	998±255	136±43	0.25	303±102	711±250	893±310	122±36	0.22	−10.6
Cedrus libani	334	267±88	622±217	782±269	107±47	0.16	248±79	576±194	725±240	99±40	0.15	−6.8
Juniperus excelsa	610	266±86	621±212	781±263	106±47	0.06	258±89	600±218	755±270	103±41	0.06	−3.0
Mixed forest	1517	252±80	585±195	737±242	101±43	0.03	199±71	455±174	576±216	79±36	0.02	−21.9
Cropland	5918	106±55	227±135	292±168	41±25	0.24	102±55	216±135	279±167	39±23	0.23	−4.4
Grassland	7385	191±30	435±73	551±90	75±19	0.55	179±28	406±72	515±88	71±14	0.52	−6.0

Based on a total of 88 flux sites, an overall mean NEP of the Asian forests was estimated at 274 ± 207 g C m^{-2} years^{-1} (Chen et al. 2013) which is about 2.5 times higher than that (110 ± 15 g C m^{-2} years^{-1}) of the Mediterranean evergreen needleleaf forests in this study. This difference is most likely to stem from biogeoclimatically broad coverage of different Asian forest ecosystems. Luyssaert et al. (2010) reported mean NEP estimates of the EU-25 forests ranging from 19 ± 6 g C m^{-2} years^{-1} by LPJ-DGVM (Sitch et al. 2003) to 200 ± 52 g C m^{-2} years^{-1} by site studies. Powell et al. (2008) estimated an annual NEP for naturally regenerated mixed stands of longleaf pine (*Pinus palustris* Mill.) and slash pine (*Pinus elliottii* var. *elliottii* Engelm.) in the range of 158 to 192 g C m^{-2} years^{-1} after 4 years of eddy covariance measurements in north Florida (MAP=1228 mm; MAT=19 °C). AmeriFlux data-derived NEP for Mediterranean evergreen forest (*Adenostoma* sp. and *Ceanothus* sp.) of Sky Oaks in California (USA) (MAP=491 mm; MAT=12.2 °C) was found to vary between 60 and 67 g C m^{-2} years^{-1} depending on the stand age (Falge et al. 2002). Nine years of eddy covariance measurements over an evergreen Mediterranean forest (*Quercus ilex*) in southern France (MAP=907 mm; MAT=13.5 °C) led to NEP values of 149 to 451 g C m^{-2} years^{-1} (Allard et al. 2008). NEP estimates of Mediterranean forests were 70 g C m^{-2} years^{-1} for *Q. ilex* forest in Italy (MAP=588 mm; MAT=15.9 °C) (Miglietta and Peressotti 1999), between 20 and 140 g C m^{-2} years^{-1} for mixed *Q. ilex* and *Q. suber* forest in Portugal (MAP=669 mm; MAT=16 °C) (Pereira et al. 2007), and between 56 and 115 g C m^{-2} years^{-1} for *Quercus douglasii* forest in California (USA) (MAP=562 mm; MAT=16.5 °C) (Ma et al. 2007).

Mean grassland NEP estimate of 75 ± 19 g C m^{-2} years^{-1} over the study region in the present climate declined by 6 % to 71 ± 14 g C m^{-2} years^{-1} in response to climate change in the 2070s. Maximum source and sink (NEP) values of C3 grasslands globally were estimated to range from −300 to 500 g C m^{-2} years^{-1}, respectively, based on a decade of eddy covariance measurements (Peichl et al. 2013). Schulze et al. (2010) quantified the mean NEP of the European grasslands as 57 ± 34 g C m^{-2} years^{-1} from flux tower measurements. On average, Peichl et al. (2013) quantified grassland NEP as 222 ± 104 g C m^{-2} years^{-1} for the maritime climate, 64 ± 70 g C m^{-2} years^{-1} for the Mediterranean climate and 60 ± 98 g C m^{-2} years^{-1} for cold-temperate climate. Ma et al. (2007) reported that long-term eddy covariance-based NEP values for the Mediterranean grassland in California (USA) (MAP=562 mm; MAT=16.5 °C) changed from a net sink of 88 ± 61 g C m^{-2} years^{-1} to a net source of -189 ± 51 g C m^{-2} years^{-1} between 2000 and 2006. A grazed Mediterranean C3/C4 grassland in southern Portugal (MAP=669 mm; MAT=15.5 °C) acted as a net source of −49 g C m^{-2} years^{-1} between 2004 and 2005 and as a net sink of 190 g C m^{-2} years^{-1} between 2005 and 2006 (Aires et al. 2008). Eddy covariance measurements of grassland NEP in the Little Washita watershed of southwest Oklahoma (USA) (MAP=760 mm; MAT=16 °C) under the climate conditions very similar to that of the upper Seyhan watershed resulted in NEP values of 41 and 118 g C m^{-2} years^{-1} in the growing seasons of 1996 and 1997, respectively (Falge et al. 2002). Multiple-year eddy covariance observations for different crops showed croplands to have mean annual NEP values ranging from 34 to 193 g C m^{-2} years^{-1} (Anthoni et al. 2004; Aubinet et al. 2009).

Total C pool of the entire terrestrial ecosystems in the upper Seyhan watershed was estimated at 1.36 Megatons (Mt) C year^{-1} (Mt=10^{12} g). The projection of regional climate change in the 2070s showed an overall decrease in the terrestrial NEP of the study region which was the most dramatic (−21.9 %) for the mixed forest (Table 4). Globally, grassland covers 20 to 40 % (26.8 to 56 million km^2) of the world's land area depending on the grassland definition and is a significant component of the global C cycle (Suttie et al. 2005). Similarly, covering 40 % of the total land area and having the largest contribution (0.55 Mt C year^{-1}) to total C pool (1.36 Mt C year^{-1}) of the study region, grassland played the most significant role in the local C cycle of the watershed for the present and future climate.

Unlike NEP, net biome production (NBP) takes into account human-induced losses and gains of ecosystem C, and hence, better represents the net amount of atmospheric CO$_2$ sequestered in ecosystem components such as vegetation and soil in the long-term. As a function of the mean forest NPP (916 ± 124 g C m^{-2} years^{-1}) in the study region, and the mean C sequestration ratio of NBP to NPP for the EU-25 forests (0.15 ± 0.05) by Luyssaert et al. (2010), the mean NBP value of the Mediterranean evergreen needleleaf forests was estimated at 137 ± 19 g C m^{-2} years^{-1} under the present climate and 124 ± 20 g C m^{-2} years^{-1} under the future climate. The mean present and future forest NBP estimates of this study

are within the European forest NBP between 70 and 160 g C m^{-2} years^{-1} (Janssens et al. 2003). The mean cropland and grassland NBP of the study region was estimated at 10±6 and 81±13 g C m^{-2} years^{-1} based on the maximum and mean ratios of NBP to NPP for the EU-25 cropland (0.03) and grassland (0.13) as presented by Ciais et al. (2010), respectively. As close to the mean cropland NBP in this study, the ORCHIDEE-STICS model (Gervois et al. 2008) provided a mean NBP estimate of 15±15 g C m^{-2} years^{-1} for the EU-25 cropland over the period of 1990 to 1999. Soussana et al. (2007) inferred a mean grassland NBP estimate of 104±73 g C m^{-2} years^{-1} (in the range of 12 g C m^{-2} years^{-1} in Hungary to 1479 g C m^{-2} years^{-1} in Denmark) from nine sites along a major climatic gradient over Europe for 2 years (MAP=500 mm in Hungary to 1313 mm in France; MAT=6.3 °C in Italy to 10.5 °C in Hungary). The mean NBP values of the three main Mediterranean ecosystems (evergreen needleleaf forest, cropland, and grassland) and their corresponding land coverage give a watershed-scale NBP estimate of 1.34 Tg C year^{-1} in this study (Tg=10^{12} g). This watershed-scale NBP estimate corresponds to 0.048, 0.079, 0.168, and 0.498 % of the total global (2.8 Pg C year^{-1}), Eurasia (1.7 Pg C year^{-1}), North America (0.8 Pg C year^{-1}), and EU-25 (270 Tg C year^{-1}) terrestrial NBP values, respectively (Schimel et al. 2001; Schulze et al. 2010) (Pg=10^{15} g).

It is clear from the above discussion that all our watershed-scale estimates about aboveground litterfall, R_H, NPP, NEP, and NBP of the terrestrial Mediterranean ecosystems fall within a reasonable range of the existing studies. The use of Envisat MERIS data in the CASA model appeared to predict spatiotemporal dynamics of C cycle at a high spatial resolution better than that of multitemporal images with a coarse-to-moderate spatial resolution such as MODIS (Nemani et al. 2009) and AVHRR (Kennedy et al. 2009). However, uncertainties associated with the estimates of the present study stem from other controls on C cycle that were not taken into account such as herbivory, management practices, non-uniform disturbance regimes including land use/cover conversions, and/or atmospheric aerosol loadings. A better understanding of the impact of these controls on terrestrial C cycle is required to reduce uncertainties with the quantification of spatiotemporal dynamics of ecosystem C gain and loss. For example, consumption of NPP by herbivory was reported to account generally for less than 10 % of NPP in forests, except when insect outbreaks may consume 50 % of NPP (Schowalter et al. 1986). Carbon sink/source capacity of ecosystems also depends on local management practices and land use strategies such as conservation tillage and residue practices, and retention of old-growth forests and understory vegetation (Wali et al. 1999; Evrendilek and Wali 2004). Chen and Zhuang (2014) found that the atmospheric aerosol loading enhanced GPP (130.0±4.1 Pg C year^{-1}), R_A (66.5±0.6 Pg C year^{-1}), R_H (52.1±1.8 Pg C year^{-1}), NPP (63.5±3.6 Pg C year^{-1}) and NEP (11.4± 4.5 Pg C year^{-1}) of the global terrestrial ecosystem over the period of 2003 to 2010 relative to the baseline values (without the effect of the aerosol loadings on C cycle) of GPP (125.1±5.2 Pg C year^{-1}), R_A (65.4±1.0 Pg C year^{-1}), R_H (52.2±2.0 Pg C year^{-1}), NPP (59.7±4.3 Pg C year^{-1}), and NEP (7.5±4.7 Pg C year^{-1}).

Conclusions

The Mediterranean ecosystems are one of the hot spots of the earth due to their supply of life-supporting ecosystem services as well as their exposure to severe, intense, and prolonged human-induced disturbances. High-resolution and meso-scale monitoring studies are needed for tailoring environmental management strategies towards strengthening C sink status of the Mediterranean ecosystems. Satellite-based ecosystem modeling with Envisat MERIS and IKONOS data proved to be promising in mapping C sink/source patterns and in capturing high variability of the Mediterranean conditions in response to regional climate change in the 2070s. Simulation estimates of C budget components in this study agreed well with observations and estimates of the related literature within their respective error bounds. With the climate change in the 2070s, a watershed-scale mean decrease was inferred in C input to the soil from aboveground litterfall by 9.0 %, BNPP by 9.7 %, ANPP by10.2 %, RH by 9.4 %, NEP by 9.1 %, and NBP by 10.1 % relative to the present climate conditions. Water limitation appears to be the main driver of the decrease of different magnitudes in NEP patterns of the study region except in northern highland regions where evapotranspiration rates are not the main limiting factor. As far as uncertainty associated with the regional C model projections is concerned, the implications of using the latest IPCC AR5 climate scenarios including improvements in representing clouds and radiative forcings, and land-

atmosphere feedbacks that will be approved and adopted towards the end of 2014 need to be explored for regionally modeled C flux simulations in the future studies. Likewise, satellite-observed canopy NDVI and fPAR data under future climate conditions should be used in the future studies since vegetation structure, and canopy cover are responsive to climate change.

Conflict of interest   The authors declare that they have no conflict of interest.

References

Aires, L., Pio, C., & Pereira, J. (2008). Carbon dioxide exchange above a Mediterranean C3/C4 grassland during two climatologically contrasting years. *Global Change Biology, 14*, 539–555.

Allard, V., Ourcival, J. M., Rambal, S., Joffre, R., & Rocheteau, A. (2008). Seasonal and annual variation of carbon exchange in an evergreen Mediterranean forest in southern France. *Global Change Biology, 14*, 714–725.

Anthoni, P. M., Freibauer, A., Kolle, O., & Schulze, E. D. (2004). Winter wheat carbon exchange in Thuringia, Germany. *Agricultural and Forest Meteorology, 121*, 55–67.

Asner, G. P., Archer, S., & Hughes, R. F. (2003). Net changes in regional woody vegetation cover and carbon storage in Texas drylands, 1937–1999. *Global Change Biology, 9*, 316–335.

Aubinet, M., Moureaux, C., Bodson, B., Dufranne, D., Heinesch, B., Suleau, M., et al. (2009). Carbon sequestration by a crop over a 4-year sugar beet/winter wheat/seed potato/winter wheat rotation cycle. *Agricultural and Forest Meteorology, 149*, 407–418.

Barford, C. C., Wofsy, S. C., Goulden, M. L., Munger, J. W., Pyle, E. H., Urbanski, S. P., et al. (2001). Factors controlling long- and short-term sequestration of atmospheric CO₂ in a mid-latitude forest. *Science, 294*, 1688–1691.

Chen, M., & Zhuang, Q. (2014). Evaluating aerosol direct radiative effects on global terrestrial ecosystem carbon dynamics from 2003 to 2010. *Tellus, B66*, 21808.

Chen, Z., Yu, G., Ge, J., Sun, X., Hirano, T., Saigusa, N., et al. (2013). Temperature and precipitation control of the spatial variation of terrestrial ecosystem carbon exchange in the Asian region. *Agricultural and Forest Meteorology, 182–183*, 266–276.

Chun-Jiang, L., Ilvesniemi, H., Berg, B., Kutsch, W., Yu-Sheng, Y., Xiang-Qing, M., et al. (2003). Aboveground litterfall in Eurasian forests. *Journal of Forestry Research, 14*, 27–34.

Ciais, P., Wattenbach, M., Vuichard, N., Smith, P., Piao, S. L., Don, A., et al. (2010). The European carbon balance. part 2: croplands. *Global Change Biology, 16*, 1409–1428.

Dash, J., & Curran, P. J. (2006). Relationship between herbicide concentration during the 1960s and 1970s and the contemporary MERIS terrestrial chlorophyll index (MTCI) for southern Vietnam. *International Journal of Geographical Information Science, 20*, 929–939.

Donmez, C., Berberoglu, S., Erdogan, M. A., Tanriover, A. A., & Cilek, A. (2015). Response of the regression tree model to high resolution remote sensing data for predicting percent tree cover in a Mediterranean ecosystem. *Environmental Monitoring & Assessment, 187*, 4 (in press).

Eswaran, H., Berberoglu, S., Cangir, C., Boyraz, D., Zucca, C., Ozevren, E., et al. (2011). *The anthroscape approach in sustainable land use, sustainable land management: learning from the past for the future*. New York: Springer.

Evrendilek, F. (2014). Modeling net ecosystem CO₂ exchange using temporal neural networks after wavelet denoising. *Geographical Analysis, 46*, 37–52.

Evrendilek, F., & Wali, M. K. (2004). Changing global climate: historical carbon and nitrogen budgets and projected responses of Ohio's cropland ecosystems. *Ecosystems, 7*, 381–392.

Evrendilek, F., Berberoglu, S., Taskinsu-Meydan, S., & Yilmaz, E. (2006). Quantifying carbon budgets of conifer Mediterranean forest ecosystems, Turkey. *Environmental Monitoring & Assessment, 119*, 527–543.

Falge, E., Baldocchi, D., Tenhunen, J., Aubinet, M., Bakwin, P., Berbigier, P., et al. (2002). Seasonality of ecosystem respiration and gross primary production as derived from FLUXNET measurements. *Agricultural and Forest Meteorology, 113*, 53–74.

Field, C. B., Randerson, J. T., & Malmstrom, C. M. (1995). Global net primary production: combining ecology and remote sensing. *Remote Sensing of Environment, 51*, 74–88.

Gervois, S., Ciais, P., Noblet-Ducoudre, N., Brisson, N., Vuichard, N., & Viovy, N. (2008). The carbon and water balance of European croplands throughout the 20th century. *Global Biogeochemical Cycles, 22*, GB2022.

Giardina, C. P., Ryan, M. G., Binkley, D., & Fownes, J. H. (2003). Primary production and carbon allocation in relation to nutrient supply in a tropical experimental forest. *Global Change Biology, 9*, 1438–1450.

Goetz, S. J., Prince, S. D., Goward, N. S., Thawley, M. M., & Small, J. (1999). Satellite remote sensing of primary production: an improved production efficiency modeling approach. *Ecological Modeling, 122*, 239–255.

Grant, R. F., Baldocchi, D. D., & Ma, S. (2012). Ecological controls on net ecosystem productivity of a seasonally dry annual grassland under current and future climates: modelling with Ecosys. *Agricultural and Forest Meteorology, 152*, 189–200.

Haberl, H., Erb, K. H., Krausmann, F., Gaube, V., Bondeau, A., Plutzar, C., et al. (2007). Quantifying and mapping the human appropriation of net primary production in Earth's terrestrial ecosystems. *Proceedings of the National Academy of Sciences of the United States of America, 104*, 12942–12945.

Haxeltine, A., & Prentice, I. C. (1996). BIOME3: an equilibrium biosphere model based on ecophysiological constraints, resource availability and competition among plant functional types. *Global Biogeochemical Cycles, 10*, 693–709.

Helsel, D. R., & Hirsch, R. M. (1992). *Statistical methods in water resources*. Amsterdam: Elsevier.

Hickler, T., Smith, B., Sykes, M. T., Davis, M., Sugita, S., & Walker, K. (2004). Using a generalized vegetation model to simulate vegetation dynamics in northeastern USA. *Ecology, 85*, 519–530.

Hollinger, D. Y., Aber, J., Dail, B., Davidson, E. A., Goltz, S. M., Hughes, H., et al. (2004). Spatial and temporal variability in forest-atmosphere CO_2 exchange. *Global Change Biology, 10*, 1689–1706.

IPCC. (2000). *Special report on emissions scenarios*. Cambridge: Cambridge University Press.

Janssens, I. A., Freibauer, A., Ciais, P., Smith, P., Nabuurs, G. J., Folberth, G., et al. (2003). Europe's terrestrial biosphere absorbs 7 to 12 % of European anthropogenic CO_2 emissions. *Science, 300*, 1538–1542.

Jian-Bing, W., Du-Ning, X., Xing-Yi, Z., Xiu-Zhen, L., & Xiao-Yu, L. (2006). Spatial variability of soil organic carbon in relation to environmental factors of a typical small watershed in the Black Soil region, Northeast China. *Environmental Monitoring & Assessment, 121*, 597–613.

Kennedy, R. E., Townsend, P. A., Gross, J. E., Cohen, W. B., Bolstad, P., Wang, Y. Q., et al. (2009). Remote sensing change detection tools for natural resource managers: understanding concepts and tradeoffs in the design of landscape monitoring projects. *Remote Sensing of Environment, 113*, 1382–1396.

Kimura, F., Kitoh, A., Sumi, A., Asanuma, J., & Yatagai, A. (2007). *Downscaling of the global warming projections to Turkey*. The Final Report of ICCAP (Impact of Climate Changes on Agricultural Production System in Arid Areas), Research Institute for Humanity and Nature.

Kirschbaum, M. U. F. (1995). The temperature dependence of soil organic matter decomposition and the effect of global warming on soil organic carbon storage. *Soil Biology & Biochemistry, 27*, 753–760.

Knapp, A. K., Burns, C. E., Fynn, R. W., Kirkman, K. P., Morris, C. D., & Smith, M. D. (2006). Convergence and contingency in production–precipitation relationships in North American and South African C4 grasslands. *Oecologia, 149*, 456–464.

Knorr, W., & Heimann, M. (1995). Impact of drought stress and other factors on seasonal land biosphere CO_2 exchange studied through an atmospheric tracer transport model. *Tellus, 47*, 471–489.

Krinner, G., Viovy, N., de Noblet-Ducoudré, N., Ogée, J., Polcher, J., Friedlingstein, P., et al. (2005). A dynamic global vegetation model for studies of the coupled atmosphere-biosphere system. *Global Biogeochemical Cycles, 19*, GB1015.

Lieth, H., & Whittaker, R. (1975). *Primary productivity of the biosphere*. New York: Springer.

Lobell, D. B., Hicke, J. A., Asner, G. P., Field, C. B., Tucker, C. J., & Los, S. O. (2002). Satellite estimates of productivity and light use efficiency in United States agriculture, 1982–1998. *Global Change Biology, 8*, 722–735.

Luyssaert, S., Inglima, I., Jung, M., Richardson, A. D., Reichsteins, M., Papale, D., et al. (2007). CO_2 balance of boreal, temperate, and tropical forests derived from a global database. *Global Change Biology, 13*, 2509–2537.

Luyssaert, S., Ciais, P., Piao, S. L., Schulze, E.-D., Jung, M., Zaehle, S., et al. (2010). The European carbon balance. Part 3: forests. *Global Change Biology, 16*, 1429–1450.

Ma, S., Baldocchi, D. D., Xu, L., & Hehn, T. (2007). Inter-annual variability in carbon dioxide exchange of an oak/grassna and open grassland in California. *Agricultural and Forest Meteorology, 147*, 157–171.

Matala, J., Kellomäki, S., & Nuutinen, T. (2008). Litterfall in relation to volume growth of trees: analysis based on literature. *Scandinavian Journal of Forest Research, 23*, 194–202.

McGuire, A. D., Sitch, S., Clein, J. S., Dargaville, R., Esser, G., Foley, J., et al. (2001). Carbon balance of the terrestrial biosphere in the twentieth century: analyses of CO_2, climate and land-use effects with four process-based ecosystem models. *Global Biogeochemical Cycles, 15*, 183–206.

Miglietta, F., & Peressotti, A. (1999). Summer drought reduces carbon fluxes in Mediterranean forest. *Global Change Newsletter, 39*, 15–16.

Nemani, R., Hashimoto, H., Votava, P., Melton, F., Wang, W., Michaelis, A., et al. (2009). Monitoring and forecasting ecosystem dynamics using the terrestrial observation and prediction system (TOPS). *Remote Sensing of Environment, 113*, 1497–1509.

Nunes, L., Lopes, D., Castro, R. F., & Gower, S. T. (2013). Aboveground biomass and net primary production of pine, oak and mixed pine–oak forests on the Vila Real district, Portugal. *Forest Ecology & Management, 305*, 38–47.

Pandey, D., Agrawal, M., & Pandey, J. S. (2011). Carbon footprint: current methods of estimation. *Environmental Monitoring & Assessment, 178*, 135–160.

Parton, W. J., Scurlock, J. M. O., & Ojima, D. S. (1993). Observations and modeling of biomass and soil organic matter dynamics for the grassland biome worldwide. *Global Biogeochemical Cycles, 7*, 785–809.

Peichl, M., Sonnentag, O., Wohlfahrt, G., Flanagan, L. B., Baldocchi, D. D., Kiely, G., et al. (2013). Convergence of potential net ecosystem production among contrasting C3 grasslands. *Ecology Letters, 16*, 502–512.

Pereira, J. S., Mateus, J. A., Aires, L. M., Pita, G., Pio, C., David, J. S., et al. (2007). Net ecosystem carbon exchange in three contrasting Mediterranean ecosystems—the effect of drought. *Biogeosciences, 4*, 1–12.

Potter, C. S., Randerson, J. T., Field, C. B., Matson, P. A., Vitousek, P. M., Mooney, H. A., et al. (1993). Terrestrial ecosystem production: a process model based on global satellite and surface data. *Global Biogeochemical Cycles, 7*, 811–841.

Potter, C. S., Klooster, S., Myneni, R., Genovese, V., Tan, P. N., & Kumar, V. (2003). Continental-scale comparisons of terrestrial carbon sinks estimated from satellite data and ecosystem modeling 1982–1998. *Global and Planetary Change, 39*, 201–213.

Powell, H. L., Gholz, K. L., Clark, G., Starr, W. P., Cropper, J. R., & Martin, T. A. (2008). Carbon exchange of a mature, naturally regenerated pine forest in North Florida. *Global Change Biology, 14*, 2523–2538.

Prince, S. D., & Goward, S. N. (1995). Global net primary production: a remote sensing approach. *Journal of Biogeography, 22*, 815–835.

Raich, J. W., & Nadelhoffer, K. J. (1989). Belowground carbon allocation in forest ecosystems: global trends. *Ecology, 70*, 1346–1354.

Raich, J. W., & Schlesinger, W. H. (1992). The global carbon dioxide flux in soil respiration and its relationship to vegetation and climate. *Tellus, B44*, 81–99.

Ruimy, A., Saugier, B., & Dedieu, G. (1994). Methodology for the estimation of terrestrial net primary production from remotely sensed data. *Journal of Geophysical Research, 99*, 5263–5283.

Ruimy, A., Dedieu, G., & Saugier, B. (1996). TURC: a diagnostic model of continental gross primary productivity and net primary productivity. *Global Biogeochemical Cycles, 10*, 269–286.

Running, S. W., Baldocchi, D. D., Turner, D. P., Gower, S. T., Bakwin, P. S., & Hibbard, K. A. (1999). A global terrestrial monitoring network integrating tower fluxes, flask sampling, ecosystem modeling and EOS satellite data. *Remote Sensing of Environment, 70*, 108–127.

Running, S., Ramakrishna, R., Nemani, F., Heinsch, A., Maosheng, Z., Reeves, M., et al. (2004). A continuous satellite-derived measure of global terrestrial primary production. *BioScience, 54*, 547–560.

Schimel, D. S., House, J. I., Hibbard, K. A., Bousquet, P., Ciais, P., Peylin, P., et al. (2001). Recent patterns and mechanisms of carbon exchange by terrestrial ecosystems. *Nature, 414*, 169–172.

Schnell, S., Altrell, D., Stahl, G., & Kleinn, C. (2014). The contribution of trees outside forests to national tree biomass and carbon stocks—a comparative study across three continents. *Environmental Monitoring & Assessment, 187*, 4197.

Schowalter, T. D., Hargrove, W. W., & Crossley, D. A. (1986). Herbivory in forested ecosystems. *Annual Review of Entomology, 31*, 177–196.

Schulze, E. D., Ciais, P., Luyssaert, S., Schrumpf, M., Janssens, I. A., Thiruchittampalam, B., et al. (2010). The European carbon balance: part 4: integration of carbon and other trace-gas fluxes. *Global Change Biology, 16*, 1451–1469.

Sellers, P. J., Randall, D. A., & Collatz, G. J. (1996). A revised land surface parameterization (SiB2) for atmospheric GCMs: part I: model formulation. *Journal of Climate, 9*, 676–705.

Sitch, S., Smith, B., Prentice, I. C., Arneth, A., Bondeau, A., Cramer, W., et al. (2003). Evaluation of ecosystem dynamics, plant geography and terrestrial carbon cycling in the LPJ dynamic global vegetation model. *Global Change Biology, 9*, 161–185.

Soussana, J. F., Allard, V., Pilegaard, K., Ambus, P., Amman, C., Campbell, C., et al. (2007). Full accounting of the greenhouse gas (CO_2, N_2O, CH_4) budget of nine European grassland sites. *Agriculture, Ecosystems & Environment, 121*, 121–134.

Suttie, J. M., Reynolds, S. G., & Batello, C. (2005). *Grasslands of the world*. FAO Plant Production and Protection Series, FAO.

Wali, M. K., Evrendilek, F., West, T., Watts, S., Pant, D., Gibbs, H., et al. (1999). Assessing terrestrial ecosystem sustainability: usefulness of regional carbon and nitrogen models. *Nature & Resources, 35*, 20–33.

Wang, W., & Fang, J. (2009). Soil respiration and human effects on global grasslands. *Global and Planetary Change, 67*, 20–28.

Wang, X., Liu, L., Piao, S., Janssens, I. A., Tang, J., Liu, W., et al. (2014). Soil respiration under climate warming: differential response of heterotrophic and autotrophic respiration. *Global Change Biology, 20*, 3229–3237.

Weiss, M., Baret, F., Pavageau, K., Béal, D., Berthelot, B., & Regner, P. (2006). *Top of canopy land products* (TOA_VEG). Contract ESA AO/1-4233/02/I-LG.

White, A. M., Thornton, P. E., Running, S. W., & Nemani, R. R. (2000). Parameterization and sensitivity analysis of the BIOME-BGC terrestrial ecosystem model: net primary production controls. *Earth Interactions, 4*, 85.

Woodward, F. I., Smith, T. M., & Emanuel, W. R. (1995). A global land primary productivity and phytogeography model. *Global Biogeochemical Cycles, 9*(471), 490.

Zaehle, S., Sitch, S., Prentice, I. C., Liski, J., Cramer, W., Erhard, M., et al. (2006). The importance of age-related decline in forest NPP for modeling regional carbon balances. *Ecological Applications, 16*, 1555–1574.

Zhao, M., Heinsch, F. A., Nemani, R. R., & Running, S. W. (2005). Improvements of the MODIS terrestrial gross and net primary production global data set. *Remote Sensing of Environment, 95*, 164–176.